GCAGS JOURNAL
A Publication of the Gulf Coast Association of Geological Societies
www.gcags.org

MICROPORES IN CARBONATE MUD: EARLY DEVELOPMENT AND PETROPHYSICS

F. Jerry Lucia and Robert G. Loucks

Bureau of Economic Geology, Jackson School of Geosciences, University of Texas at Austin, Austin, Texas 78713, U.S.A.

ABSTRACT

Micropores are commonly found in mud-dominated fabrics located between microspar and microrhombic calcite. Understanding the development of micropores is important in petroleum geology to facilitate predicting its distribution and reservoir properties in carbonate reservoirs. The diagenetic history of micropore development can be long and complex. Many geologists have emphasized dissolution of low-porosity micrite as the principal process in forming micropores, whereas others have emphasized simple cementation of depositional carbonate mud. This study is focused on the early transformation of a depositional lime mud to a microporous microspar fabric. The material used in this study is from the core taken from well Clino on the western slope of the Great Bahama Bank. Previous investigations of this transformation have concluded that microspar is cemented aragonitic sediment. Results of our study suggest that the initial phase of the transformation is a replacement process with dissolution of micrometer- to nanometer-sized aragonitic/calcitic precursor sediment and precipitation of 1- to 10-micron microspar crystals. No porosity is gained or lost during this process indicating that no carbonate is added to or subtracted from the system. Carbonate is added later in the form of porosity reducing cement. The increase in crystal size has a strong impact on permeability by increasing permeability tenfold without changing porosity.

INTRODUCTION

Large volumes of micropores are present in many porous carbonates. Micropores in limestones are often referred to as microporosity, which is an incorrect use of the term porosity and will not be used in this report. Micropores are located within carbonate grains and between particles in carbonate mud. Microporous carbonate muds are chalks if composed of micropores between planktonic sediment or mud-dominated fabrics composed of micropores between micrite crystals. Microporous mud-dominated fabrics are a diagenetic product of depositional lime mud, whereas microporous chalks are typically made up of sedimentary particles that ranging from microns to nanometers in size. Petrophysically, porosity and permeability values of microporous lime mudplot within the petrophysical class 3 field defined by Lucia (1995), whereas microporous chalks plot below the class 3 field.

Understanding the development of micropores in mud-dominated fabrics requires understanding the diagenetic history of carbonate mud. Too often geologists conclude that micropores are formed by simple dissolution without adequately considering the precursor diagenetic history (Dravis, 1989; Jameson, 1994; Cantrell and Hagerty, 1999; Heasley et al., 2000; Lambert et al., 2006). The focus of this study is to understand the changes in texture, pore structure, porosity, and permeability that occur in the mud fraction of mud-dominated carbonates during the initial diagenetic stages.

Cores recovered from the west margin of the Great Bahama Bank (Ginsburg et al., 2001) offer an excellent opportunity to study the early development and petrophysics of micropores in mud-dominated fabrics. Of particular interest is the Clino core because (1) stable isotopes indicate a marine diagenetic environment for the Miocene and most of the Pliocene, thus eliminating the added complexity of meteoric diagenesis, (2) aragonitic muds transition downward into calcitic muds, and (3) a shift in porosity-permeability relationships accompanies that transition (Melim et al., 2001b). This study explores the reasons for the change in porosity-permeability relationships at the boundary between aragonitic and calcitic mud, as reported by Melim et al. (2001a).

GEOLOGIC SETTING

The Clino core is well described in the Society of Economic Paleontologists and Mineralogists Special Publication 70, edited by Ginsburg (2001). In 1990, two holes were drilled, logged, and cored on the western margin of Great Bahama Bank as part of the Bahama Drilling Project. Well Unda was designed to core platform sediments, and well Clino was designed to core slope sediments. This study is based on samples from the Clino core (Fig. 1). The core from well Clino sampled Pleistocene through

Manuscript received April 26, 2013; revised manuscript received May 28, 2013; manuscript accepted May 31, 2013.

GCAGS Journal, v. 2 (2013), p. 1–10.

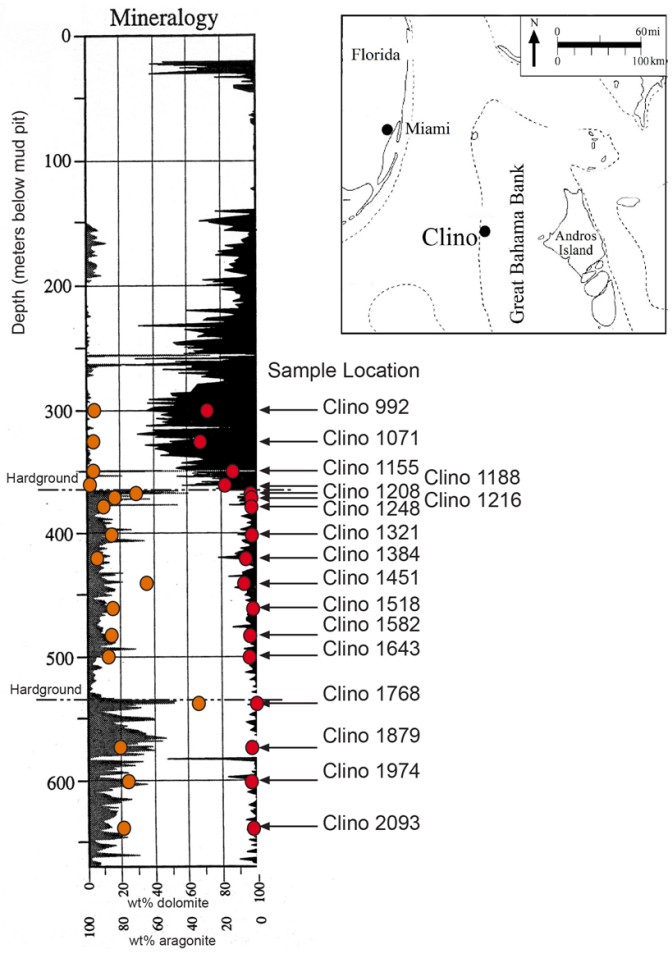

Figure 1. Depth plot showing location of samples and comparing mineralogy of current samples with that of Melim et al. (2001a). Red dots are current data. Inset is a location map for well Clino.

upper Miocene sediments, reaching a depth of 678 m (2222 ft). All depths are listed as below mud pit. The depositional history was well described by Kenter et al. (2001). The Pleistocene is reefal. Pliocene and upper Miocene sediments are slope deposits with sediment derived mainly from the shelf. The interval of interest in this study is below 300 m (984 ft), which ranges from mid-Pliocene to upper Miocene. The interval is divided by two prominent marine hardgrounds at 367.1 m (1204 ft) and 536.33 m (1770 ft) (Fig. 1). Above the first hardground, the carbonate is described as peloid lime mudstone, wackestone, packstone, and grainstone. Below the first hardground, the carbonate is described as silt- to fine-sand-sized skeletal packstone to grainstone with some wackestone. Note that the skeletal and peloidal grains are generally in the silt-sized range and the core has been characterized as monotonously muddy despite the presence of intervals of fine-grained grainstone and grain-dominated packstone. The sediment was deposited in a slope environment, and it is interpreted to have been transported off the shelf. The change in texture above and below the hardground has been correlated with a change in sediment type from skeletal to nonskeletal that occurred on the shelf during the Pliocene (Kenter et al., 2001).

DATA AND METHODS

Seventeen 1-in (2.54-cm) core plugs were collected from the Bahama Clino core drilled on the western Great Bahama Bank (Ginsburg et al., 2001) so that the relationship between porosity, permeability, and rock fabrics in this micropore-rich system could be studied. Sample depths are compared with a description of core mineralogy published by Melim et al. (2001a) (Fig. 1). The Pleistocene interval was not sampled because of the heavy overprint of meteoric diagenesis during Pleistocene sea-level fall. Sampling was concentrated in the upper Miocene to Pliocene section, where geochemical evidence indicates the presence of a marine diagenetic environment (Melim et al., 2001a). The sampling program was focused on collecting material across the transition from aragonite-rich to aragonite-poor carbonate so that changes in fabric and petrophysics could be observed.

Mineralogy was determined using x-ray diffraction (XRD) by Dr. Necip Guven at the University of Texas at San Antonio using a Rigaku-Ultima IV (2007) diffractometer (Fig. 1; Table 1). Dolomite amounts are similar to those presented by Melim et al. (2001a), and the transition from aragonitic carbonate to calcitic carbonate has the same trend. The volume of aragonite in the lower 13 samples presented in this paper is similar to that of published data.

Some aragonite amounts in the upper four samples are substantially lower than those in published data (Fig. 1). The upper two samples have 25 and 30% aragonite, respectively, whereas volume of aragonite reported by Melim et al. (2001a) is around 50%. The next lower sample has 12% aragonite compared with a published value of 40%, and the next lower sample has 16% aragonite, which is close to the value of published data. The aragonite percentages reported herein were tested by comparing grain densities measured by Weatherford Labs with reconstructed grain densities using XRD mineral percentages. Grain densities were calculated using a density of 2.93 for aragonite, 2.71 for calcite, and 2.87 for dolomite, and mineral percentages from XRD (Table 1). Calculated grain densities for the upper two samples average 2.77 gm/cc, which compares favorably with 2.75 gm/cc from core analysis. However, if 50% aragonite is used, calculated grain density is 2.82 gm/cc, which is not comparable to core grain density values. Therefore, we think that our XRD data are accurate. The reason for this disparity with published data is unknown, but is probably related to sample bias.

The 17 samples were analyzed for porosity and permeability by Weatherford Labs in Midland, Texas. Porosity was measured using a Boyles's Law Porosimeter and permeability was measured using a Hassler Permeameter. In addition, mercury injection capillary pressure (MICP) was measured on five samples by Exxon Mobil Corporation. Porosity and permeability results (Table 1) are compared with data published by Melim et al. (2001b) (Fig. 2). Published data are from a variety of sources. Porosity was obtained from neutron logs and from scattered core plugs. Permeability was measured on core plugs using a Hassler Sleeve and on core slabs using a minipermeameter. Minipermeameter data were averaged over 3-ft (1-m) intervals.

In general, new porosity and permeability values are similar to those of the published data. The published data are from a variety of scales. Permeability data are averaged minipermeameter measurements, whereas porosity data are from the neutron log. Only core-plug data from the same depth would be expected to be directly comparable. The published data between about 350 and 370 m (1148–1214 ft) has a number of plug measurements that matched our data but has five core plugs with low porosity and permeability values that do not correspond to any in our sample set (Fig. 2). However, the published plug porosity is much lower than neutron log porosity, and plug permeability is much lower than averaged minipermeameter permeability, which suggests that these plug samples were from cemented thin beds that are not sampled in this study. The low minipermeameter value at about 422 m (1384 ft) was not confirmed by the new sample 1384, which has a permeability of 10 md rather than 0.1 to 1.0 md. The low published permeability at about 442 m (1450 ft) was sampled (sample 1451), but unfortunately permeability could not be measured.

New samples show a shift from low to high permeability values at about 367 m (1204 ft), whereas porosity remains relatively constant. Published data show a similar shift in permeability. The new samples were selected to investigate the reason for this shift in permeability.

Table 1. Basic thin section descriptions, core measurements, and mineralogy. All depths are below mud pit. (GDP = grain-dominated packstone, MDP = mud-dominated packstone, Phi = porosity, Perm. = permeability, GD = grain density, Arag. = Aragonite, LMC = low magnesium calcite, Dol. = dolomite, and XRD = x-ray diffraction.)

Sample Depth		Thin Section		Core Measurements			XRD		
feet	meters	Fabric	Vugs (%)	Phi (%)	Perm. (md)	GD	Arag. (%)	LMC (%)	Dol. (%)
992	302.4	skeletal wackestone	0	42.4	2.12	2.74	25	73	2
1071	326.5	skeletal wackestone	0	42.2	1.74	2.75	30	68	2
1155	352.1	skeletal wackestone	3	38.5	6.88	2.69	12	86	2
1188	362.2	skeletal wackestone	5	38.8	3.04	2.71	16	84	0
1204	367.1	Marine Hardground							
1208	368.3	skeletal/peloid MDP	3	47.4	118.82	2.71	2	71	27
1216	370.7	skeletal/peloid MDP	10	45.1	122.41	2.68	2	83	15
1248	380.5	cemented silt-size skeletal/peloid GDP	0	17.1	2.33	2.71	2	89	9
1321	402.7	silt-size skeletal/peloid GDP	5	28.9	10.12	2.69	2	85	13
1384	422.0	skeletal/peloid wackestone	8	33.0	9.41	2.68	4	91	5
1451	444.2	skeletal wackestone	0	42.9	NA	2.71	5	60	35
1518	462.8	skeletal/peloid MDP	5	39.9	65.67	2.68	1	85	14
1582	482.3	skeletal/peloid MDP	10	46.0	78.65	2.71	2	85	13
1643	500.9	skeletal/peloid MDP	8	40.0	68.32	2.67	3	85	12
1768	539.0	silt-size skeletal/peloid GDP	5	39.0	169.01	2.72	0	34	66
1879	572.9	skeletal/peloid MDP	7	43.4	126.42	2.66	2	79	19
1974	601.8	skeletal/peloid MDP	10	40.9	179.03	2.67	1	79	23
2093	638.1	skeletal/peloid MDP	7	34.2	43.05	2.72	1	78	21

The relationship between permeability, pore-size, and rock fabrics was studied using scanning electron microscopy (SEM) images of broken surfaces and polished thin sections from the 17 samples. Standard thin sections impregnated with fluorescent blue dye were prepared for microscopic examination. Thin-section descriptions (Table 1) differ from those provided by Melim et al. (2001a, 2001b) because they used the Dunham classification, and this paper uses a modified Dunham classification that divides *packstone* into grain-dominated packstone (GDP) and mud-dominated packstone (MDP) (Lucia, 1995). Seven broken rock chips and ten polished thin sections were prepared for viewing on a field-emission FEI Nova NanoSEM 430 having a Bruker energy-dispersive spectroscopy system. Rock chips were coated with gold palladium. Polished thin sections were coated with carbon.

ROCK FABRIC—PETROPHYSICAL RELATIONSHIPS

Porosity and permeability are crossplotted and compared with standard petrophysical rock fabric class fields (Lucia, 1995) (Fig. 3). Aragonitic samples plot below the class 3 field, and calcitic samples plot in the class 3 field. Permeability has been shown to be a function of pore-throat size (Pittman, 1992), and permeability in these samples is also assumed to be related to pore-throat size. To test this assumption, five samples—two low-permeability aragonitic carbonates and three high-permeability calcitic samples—were submitted for mercury-injection capillary pressure tests to measure pore-throat sizes (Fig. 4). The average median pore-throat radius of aragonitic samples 992 and 1155 is 0.22 µm, which is within the micropore-size range. The median pore-throat radius of calcitic samples 1208 and 1974 is 2.20 µm, which is within the mesopore-size range. Calcitic sample 1384 has an intermediate pore-throat radius of 0.74 µm because porosity is reduced to 33% by calcite cement filling pores and reducing pore-throat size accordingly (Fig. 4b). Permeability and pore-throat size correlate well, as predicted (Fig. 5).

Two basic rock fabrics are considered to be present on the basis of thin-section descriptions and SEM images. The first fabric is a skeletal wackestone with micrite composed of a range of crystal sizes and shapes (Fig. 6) that is characteristic of the upper four samples. SEM photographs show this fabric to be composed of (1) elongated crystals with pointed ends ranging in size from 1 to 3 µm that are referred to as needles, (2) elongated crystals with square ends ranging in size from several micrometers to nanometers that are referred to as rods, and (3) anhedral equant crystals that are mostly in the nanometer range. This texture is referred to herein as *minimicrite* (see discussion by Folk, 1974; MacIntyre and Reed, 1995, 1998). The second fabric typically is a skeletal/peloid MDP with varying amounts of small oval vugs (Fig. 7). SEM photographs show the mud fraction dominated by 1 to 10 µm calcite crystals referred to as *microspar*. The crystal size of the microspar includes some crystals that are smaller than proposed by Folk (1965), but the average size is about 5 µm, which is consistent with Folk's definition. One to 20% remnant minimicrite is found lining pore space. Minimicrite crystals are micron- to nanometer-sized rods and anhedral crystals with few needle-shaped crystals.

Minimicrite fabric grades into microspar fabric. Thin sections show the upper four samples to be characterized by minimicrite, with a few *Globigerina* and silt-sized patches of sparry calcite thought to be recrystallized skeletal fragments (Fig. 3a). The upper two samples (992 and 1071) contain 25 to 30% aragonite, respectively. SEM backscatter photographs show a few silt-sized skeletal fragments composed of sparry calcite in a minimicrite matrix (Fig. 8a). The porosity of both samples is 42%; permeabilities average 2 md. Measured median pore-throat radius of sample 992 is 0.15 µm.

The next two samples (1155 and 1188) differ somewhat from the upper two samples. In thin section, they contain 3 to 5% oval vugs about 30 µm in diameter. They have less aragonite (12 and 16%, respectively). Note that SEM photographs show scattered 2- to 5-µm microspar crystals associated with pore space and small vugs interpreted to have formed by dissolution of minimicrite (Fig. 8b). Microspar crystal faces are euhedral.

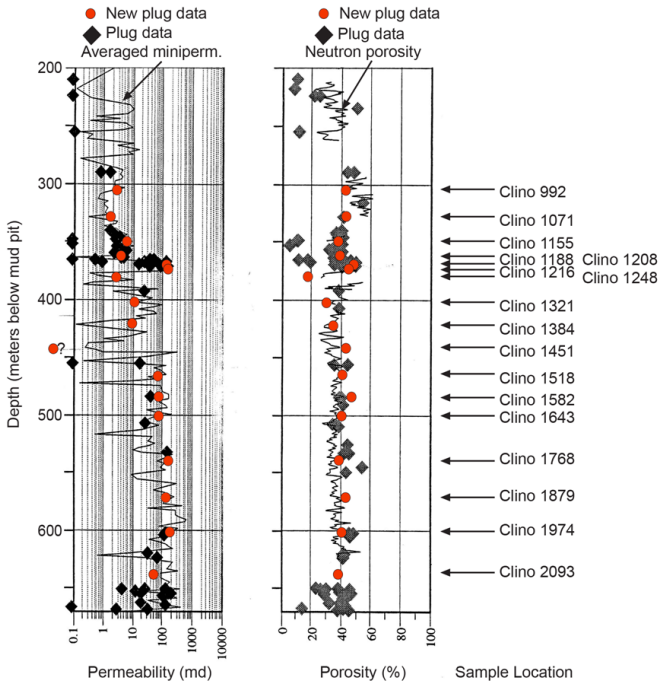

Figure 2. Depth plot showing location of samples and comparing porosity and permeability of current samples with that of Melim et al. (2001b). Red dots are current data.

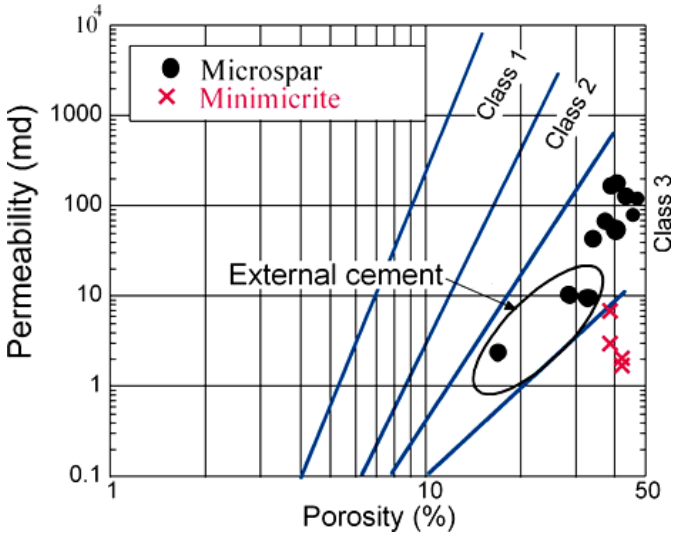

Figure 3. Cross plot of porosity and permeability illustrating difference between microspar and minimicrite samples. Microspar samples with external cement are flagged.

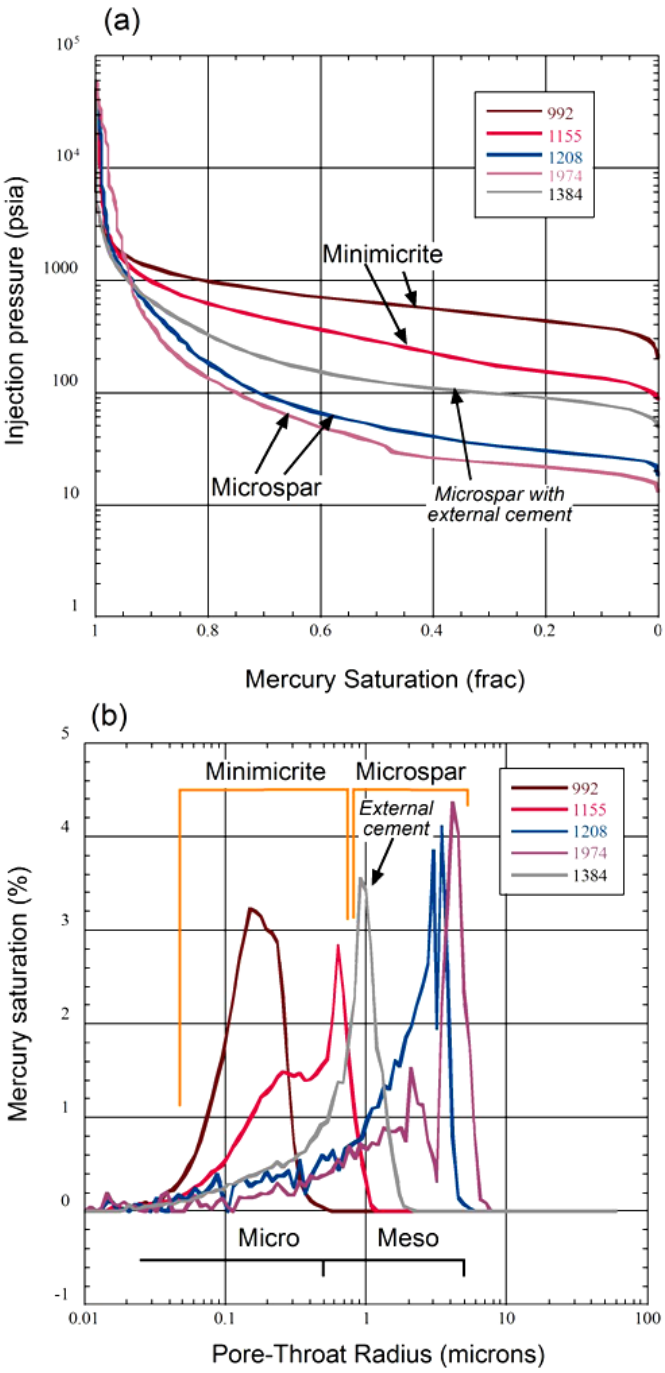

Figure 4. Mercury capillary pressure data. (a) Capillary pressure curves illustrating high entry pressures for minimicrite and lower entry pressures for microspar. (b) Distribution of pore-throat radii showing minimicrite in the micropore range and microspar in the mesopore range. However, these pores are not visible in thin section and are all considered microporosity.

Rods and needle shaped crystals have a knobby texture and some rods are cemented into slabs (Fig. 8c).

Porosity of these two samples is 38%, somewhat less than that of the upper two samples. Permeabilities are 6.88 and 3.04 md, somewhat higher than those of the upper two samples. Median pore-throat radius of sample 1155 is 0.396 µm. However, the distribution of sizes shows a range from about 0.2 to about 0.6 µm (Fig. 4), which is consistent with a dual pore system controlled by the size of minimicrite particles and the size of dissolution pores associated with microspar.

The lower 15 samples are characterized by microspar. In thin section, these samples are predominantly skeletal/peloid dolomitic MDP with up to 10% oval vugs between 30 and 50 µm in diameter (Table 1) (Fig. 7a). Two samples are skeletal dolomitic GDP, and two are skeletal dolomitic wackestones. Skeletal and peloid grains are very fine sand to silt size. XRD analysis shows the average value for calcite is 77%, that of aragonite is 3% and that of dolomite is 20%.

SEM analysis conducted on seven microspar samples shows a fabric of 1- to 10-µm microspar, with varying amounts of minimicrite, dolomite, intercrystal pore space, and small vugs (Fig. 8d). Large patches of microspar are observed, and close examination shows that they are composed of microspar crystals that

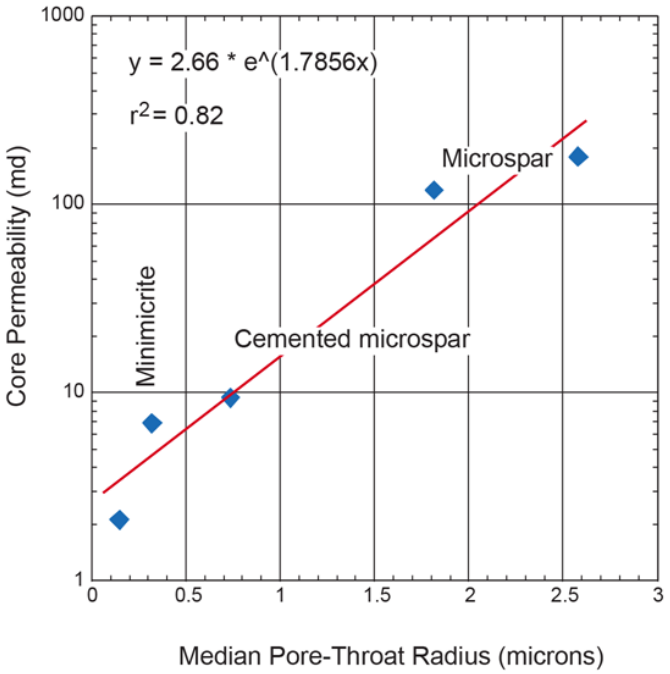

Figure 5. Cross plot of permeability and median pore-throat radius showing good positive correlation.

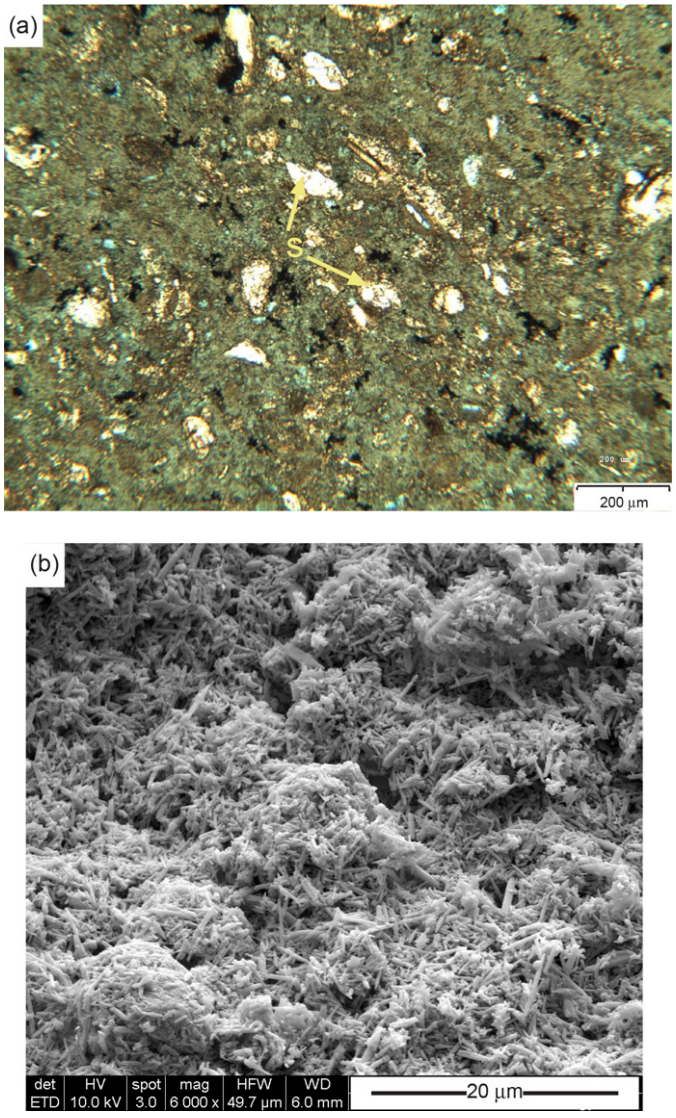

Figure 6. Clino 992. (a) Thin-section photomicrograph showing sparry calcite skeletal fragments (s) in porous lime mud (minimicrite), and (b) Broken surface SEM photograph of minimicrite composed of 75% calcite and 25% aragonite, showing texture of needles, rods, and anhedral equant crystals in micro-to-nano size range.

have coalesced (Fig. 8e). When remnant minimicrite is present, it is found lining pore space and plastered on faces of microspar (Fig. 8f). The remnant minimicrite is composed of rods and submicron, anhedral, equant crystals, and only a few needle-shaped crystals.

Visual estimates suggest that most samples contain only a small percentage of minimicrite. Samples 1384 and 1451, however, have an estimated 10 to 20% minimicrite and, interestingly, 4 to 5% aragonite, the highest percentage of aragonite in the microspar fabrics. In deeper samples, only small amounts of minimicrite remain, in the form of microrhombic calcite.

Two GDP samples, 1248 and 1321, have 17.1 and 28.6% porosity and 2.33 and 10.12 md permeability, respectively, and wackestone sample 1384 has 33% porosity and 9.41 md, much lower than average values. SEM images show large areas of microspar crystals cemented together (Fig. 9b), and thin sections of GDP show cement in intergrain pore space (Fig. 9a). These three samples illustrate the introduction of porosity-reducing calcite cement after much of the minimicrite has been transformed to microspar.

The lower 13 samples have an average porosity of 38% and an average permeability of 83 md. The median pore-throat radii of uncemented samples 1208 and 1974 are 1.81 and 2.58 µm, respectively. These values are much larger than those of the minimicrite samples and are linked to the size of microspar crystals and microspar patches. Sample 1384 has an intermediate median pore-throat radius of 0.74 µm because cementation has reduced porosity and pore size.

The conclusion from the sample descriptions is that pore-throat sizes are controlled by crystal size and porosity. Minimicrite samples have the smallest crystal size and the smallest pore-throat sizes, and the microspar samples have the largest crystal size and the largest pore-throat sizes. Conversion of minimicrite to microspar has increased pore-throat size and permeability without changing porosity.

TRANSFORMATION OF MINIMICRITE TO MICROSPAR

Because no porosity is lost, the transformation of minimicrite to microspar is not a simple cementation process. Therefore, the transformation is a replacement process. Minimicrite is dissolved and microspar precipitated locally. The initial fabric of the Pliocene-age carbonate in this dataset (McNeill et al., 2001) is composed of needles, rods, and anhedral equant calcite crystals (Figs. 6a, 6b, and 8a), and the mineralogy is between 30 and 50% aragonite, with the remainder being calcite. The exact mineralogy and fabric of the original lime mud sediment are unknown but may have been similar to current slope sediments that are 85% mud and contain between 57 and 93% aragonite (Rendel and Reijmer, 2002). Some aragonite could have recrystallized to calcite during burial and before microspar development. Burial compaction certainly reduced depositional porosity to the current porosity of the 42%, which is consistent with mechanical compaction curves for this depth (Goldhammer, 1997).

The initial stage of microspar formation as seen in this sample set is dissolution of minimicrite enlarging intercrystal pore space and local precipitation of microspar. Figure 8b shows microspar scattered in a matrix of minimicrite and small vugs juxtaposed to microspar. Minimicrite has dissolved and microspar has formed by precipitation. Some elongated and rod-shaped crystals have a knobby texture, suggesting dissolution, and some rods appear to be cemented into slabs (Fig. 8c). Crystal faces of mi-

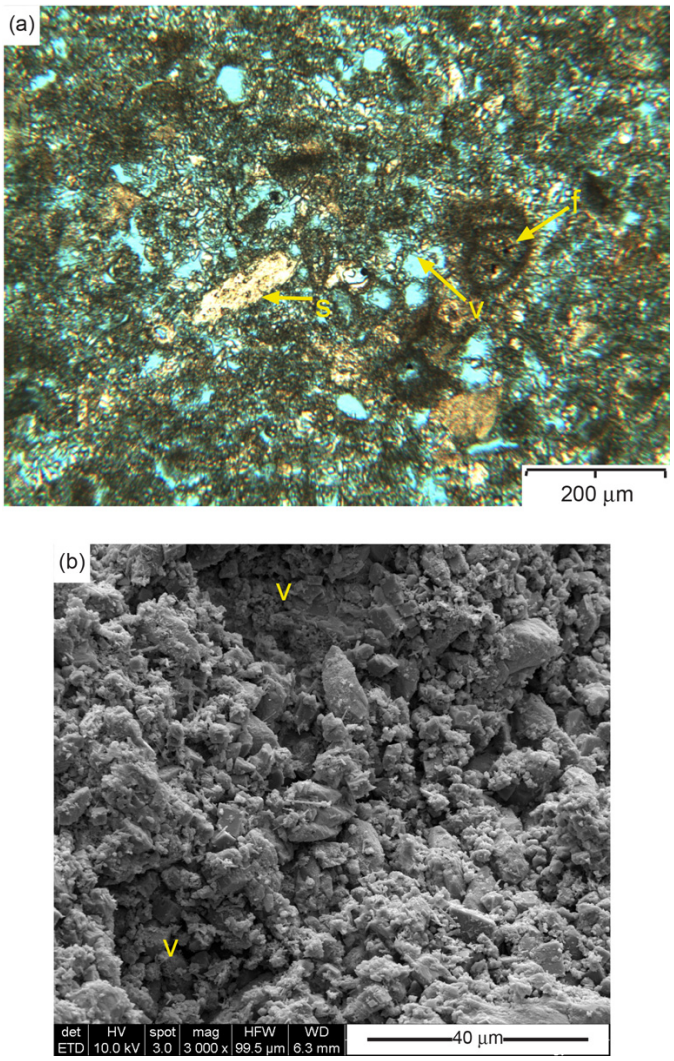

Figure 7. (a) Clino 1208. Thin-section photomicrograph showing small vugs (v), foram (f), and sparry calcite skeletal fragments (s) in porous lime mud (microspar). (b) Clino 1216. Broken surface SEM photography of microspar composed of 1- to 10-mm anhedral calcite crystals and some minimicrite plastered on crystal faces. Aragonite estimated at 2% by XRD for this sample.

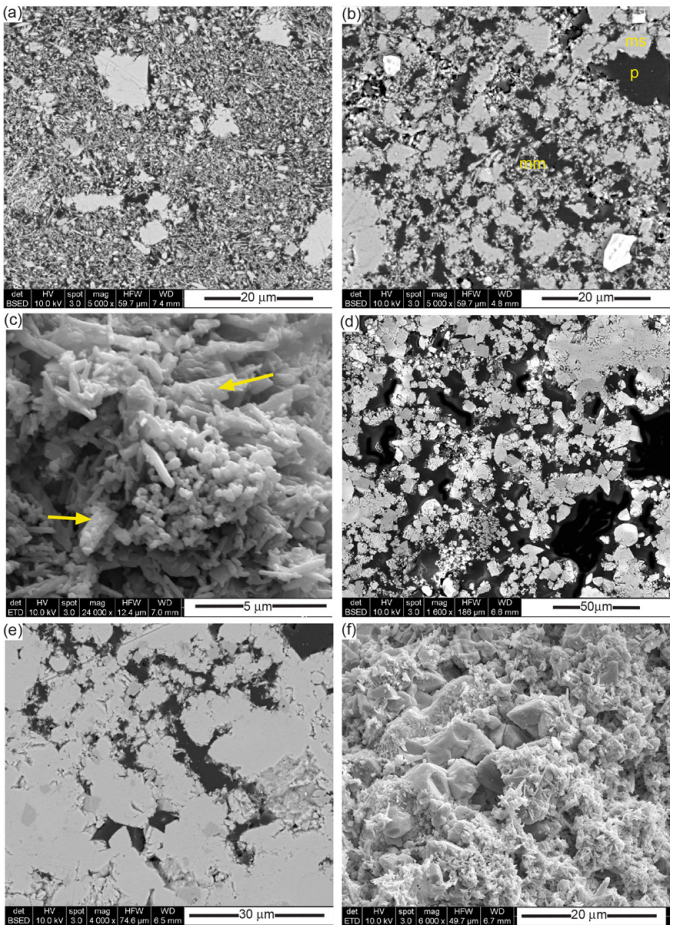

Figure 8. (a) Clino 1071. Backscatter SEM photograph showing minimicrite and a few sparry calcite skeletal fragments. (b) Clino 1188. Backscatter SEM photograph showing minimicrite (mm), scattered microspar (ms), and intermicrospar pores (p) formed by dissolution of minimicrite. Note uneven crystal faces. (c) Clino 1188. Broken surface SEM photograph showing poorly developed rods with knobby texture, slabs of cemented rods (arrows) and submicron rhombs. (d) Clino 1216. Backscatter SEM photograph showing fabric composed of microspar, intermicrospar pore space and small vugs. (e) Clino 1384. Backscatter SEM photograph showing coalescing of microspar. Note uneven crystal faces. (f) Clino 1384. Broken surface SEM photograph showing 5- to 10-mm microspar crystals with intermicrospar pores and with minimicrite coating crystal faces. Some crystal faces well developed and some poorly developed.

crospar are anhedral owing to minimicrite crystals inhibiting growth of microspar. Note that porosity remains between 42 and 38% during this initial stage of microspar formation. Presence of dissolution vugs adjacent to microspar and consistency of the porosity indicate that compaction has not offset minimicrite dissolution.

The next stage of microspar formation is a fabric composed of microspar with only a small percentage of remaining minimicrite lining pore spaces (Fig. 8d–8f). Microspar is commonly coalesced into patches of calcite (Fig. 8e). Individual microspar crystals can be seen partly cemented together, and close examination of calcite patches shows that they are composed of microspar crystals cemented together. Crystal faces are commonly uneven (Fig. 8e). The porosity of microspar samples that do not show evidence of cementation ranges from 47 to 39%. Note that the starting minimicrite fabric was converted to microspar fabric without any significant change in porosity. An increase in porosity would be expected because the molar volume of aragonite is about 8% higher than that of calcite. However, the effect of this molar volume difference is negligible because average porosity of the initial microspar is about 40% and the amount of aragonite is 50% or less.

The consistency of porosity during transformation suggests that the replacement occurred without any addition of carbonate from an outside source. However, three microspar samples have reduced porosity values and evidence of calcite filling intergrain pore space and vugs, as well as pore space between microspar crystals (Fig. 9). Therefore, the final stage is addition of carbonate from an outside source occluding pore space and reducing porosity after most minimicrite has been converted to microspar. The final result is the low-porosity microspar fabric commonly observed in mud-dominated fabrics, as described by Lasemi and Sanderg (1984).

The suggested transformation process is summarized in Figure 10. The minimicrite fabric has 40% porosity, very low permeability, and a very small pore-throat size. Carbonate from the dissolution of minimicrite is used to grow microspar, resulting in larger crystals, larger pores juxtaposed to microspar, larger pore-throat sizes, and higher permeability without a significant change

in porosity. The final stage in microspar development is a fabric of 1- to 10-µm crystals, some of which are coalesced to form patches, resulting in the highest permeability and largest pore-throat sizes. Again, there is no significant change in porosity. After formation of the microspar fabrics, addition of carbonate from an outside source reduces porosity, permeability, and pore-throat sizes. Porosity and permeability of the final fabric will depend on the volume of imported carbonate, as well as degree of burial compaction.

Interestingly, microspar crystals that formed by this process commonly have crystal faces that are uneven and anhedral (Figs. 7 and 8). Minimicrite crystals are observed on crystal faces, and the existence of anhedral crystal faces may be related to the interference of minimicrite crystals in the growth of microspar. Crystal growth appears to be retarded when existing crystals are encountered. These crystals are later dissolved to provide $CaCO_3$ for continued microspar growth, resulting in uneven crystal faces.

The textural changes observed are similar to those obtained in experimental conversion of aragonite to calcite presented by McManus and Rimstidt (1982) and Moshier and McManus (1986) and described by Moshier (1989). In these experiments, synthetic aragonite crystals were dissolved and reprecipitated as 10-µm calcite crystals.

DISCUSSION

The relationship between pore types and permeability in the Clino samples was extensively discussed by Melim et al. (2001b). They used measured permeability and porosity from 21 core plugs and minipermeameter permeability and neutron-log porosity from 101 depths. The cross plot of porosity and permeability from our 17 plugs is similar to that of their 21 plugs, except that Melim et al. (2001b) recorded more scatter and, unlike those workers, we have four samples with permeability ranging from 1 to 10 md and 40% porosity.

Macroporosity, microporosity (total porosity less macroporosity), and connected macroporosity were measured by Melim et al. (2001b) from thin sections by point counting and plotted versus permeability. They concluded that permeability is related to connectivity of macropores and that microporosity makes little contribution to permeability. MICP analysis demonstrates that primary connected pore space is basically intercrystalline and located between minimicrite crystals, microspar, and patches of microspar. Small vugs are connected through intermicrospar pore space. The connected pore space is not clearly visible in thin section and is considered to be micropores (microporosity), although the pore-throat sizes range from micro- to mesopore sizes. The difference between the low- and high-permeability samples is the increase in crystal size resulting from the transformation of minimicrite to microspar. Melim et al. (2001b) concluded that permeability is related to macroporosity, but did not attempt to relate crystal size of mud-dominated fabrics to porosity and permeability.

Melim et al. (2001b) defined macropores to include intercrystal pores, and pore space between microspars could be included in their definition. Whether microspar intercrystal pores are micropores or macropores depends on a judgment as to their visibility in thin section. We think that because they are not clearly visible in thin section, they are micropores.

The origin of microspar was discussed extensively by Folk (1965), who concluded that it forms by neomorphic crystal growth of a dense micrite. That conclusion was disproven by Lasemi and Sanderg (1984), Munnecke et al. (1997), Westphal et al. (2000), and Melim et al. (2002). These authors proposed that microspar is instead formed by cementing aragonitic sediment (sediment similar to modern sediment found on the Bahama Platform) after or during conversion of aragonite to calcite.

We agree with these authors that cementation is an important aspect of forming a microspar fabric. However, our data suggest that the initial phase of microspar formation is the replacement of minimicrite by microspar without significant change in porosity. Previous authors recognized that the formation of microspar requires some form of aragonite transformation. None of these authors, however, presented a clear method for this conversion. The model proposed by Munnecke et al. (1997) suggested that microspar crystals form as cement, engulfing aragonite needles and reducing porosity. Embedded aragonite crystals are later dissolved and filled with calcite cement. These authors proposed that microspar nucleated only on calcitic particles in the sediment, not on aragonite needles. They also recognized that it would be difficult to dissolve embedded aragonite because embedded crystals are effectively isolated from interstitial fluids. The source of the cementing carbonate was thought to be external, which would imply that the formation of microspar is a porosity-destroying mechanism. However, no substantiating porosity data were presented.

The source of cementing carbonate was addressed by Westphal et al. (2000). Their model calls for dissolution of aragonite sediment from some beds, transporting the carbonate by diffusion some distance, and cementing aragonitic sediment in other beds. In this model, porosity of the dissolved sediment is kept constant by inferred ongoing compaction. The distinction between beds of aragonite dissolution (compacted) and cemented beds (uncompacted) is based on textural observations and the concen-

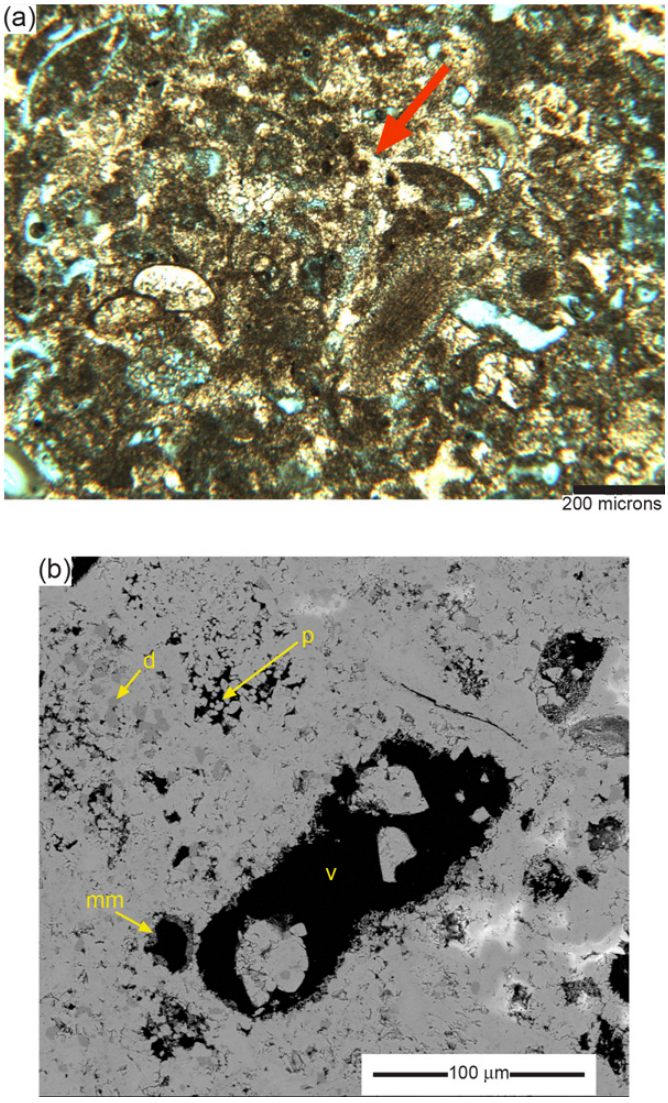

Figure 9. Clino 1248. (a) Thin-section photomicrograph of grain-dominated packstone with partly cemented intergrain pore space (arrow). Porosity is 17.1% and permeability is 2.33 md. (b) Backscatter SEM photograph showing coalesced microspar enclosing dolomite (d), pore space between microspar (p), vuggy pore space (v), and minimicrite lining vug (mm).

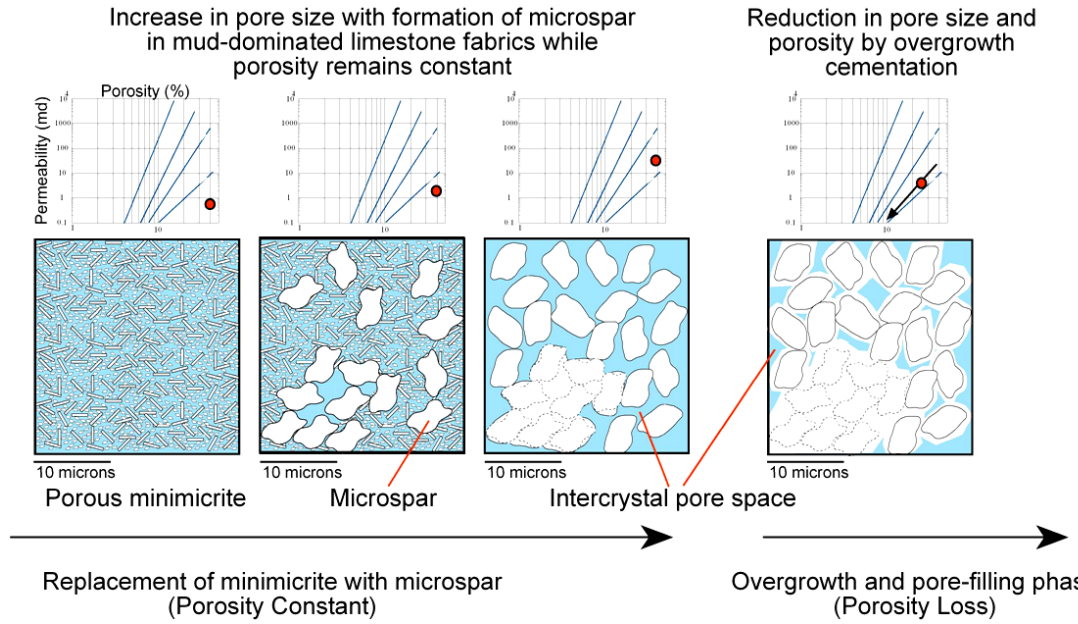

Figure 10. Diagram illustrating development of microspar fabric and associated intermicrospar pores by (1) dissolution of porous minimicrite (depositional lime mud?) and precipitation of microspar with no loss or addition of $CaCO_3$, and (2) later addition of $CaCO_3$ in the form of porosity-reducing overgrowth cement. Porosity-permeability graphs illustrate progressive change in petrophysics.

tration of palynomorphs in compacted beds. The implication is that the cemented beds have very low porosity. However, the authors did not test their model against porosity measurements, and comparing their depth plot of compacted (dissolution) and uncompacted (cemented) beds with the porosity log presented shows no consistent correlation between low porosity and uncompacted layers.

Melim et al. (2002) placed the studied interval in their closed system of marine burial diagenesis and suggested a closed system of recycling carbonate by dissolution in one location and precipitation in another. Cement found in their grainstones comes from an external source. This process is similar to the process proposed here, except our model calls for dissolution and reprecipitation on the scale of microns. These authors restated that microspar in these samples is cement.

Previous authors argued that the presence of aragonite crystal molds in microspar suggests cementation of the original sediment without a dissolution phase. By contrast, we observed minimicrite plastered on crystal faces in images of broken surfaces and uneven crystal faces that we interpreted to be places where minimicrite crystals interfered with microspar growth in backscatter images of polished sections. Unlike previous authors, we did not etch our samples to look specifically for aragonite crystal molds. However, had aragonite crystal molds been present in our polished thin sections and backscatter images, we would have expected to see evidence of them; we observed none. In addition, XRD measurements show little or no aragonite remaining in the microspar fabric. Therefore, we see no evidence that aragonite was engulfed by the microspar.

Petrophysical data support replacement of minimicrite by microspar without any significant loss of porosity. Therefore, the transformation process cannot be simple cementation. Instead, the conversion of minimicrite to microspar is a process of dissolution of less-stable aragonite and nano-sized calcite crystals, followed by local reprecipitation of more stable calcite. The presence of dissolution vugs in the partly transformed minimicrite indicates that, contrary to Westphal et al. (2000), compaction is not a major process in the transformation. Low-porosity samples are partly cemented microspar fabric, with some remnant minimicrite and little or no aragonite remaining.

More recently, Volery et al. (2009, 2010) presented a dissolution and reprecipitation model for Cretaceous microporosity that is similar to the model presented herein for Pliocene-Miocene micropores. However, they concluded that only calcitic sediment converts to microspar and that aragonitic sediments are transformed into tight micritic limestones. The data presented here show that microporous fabrics can develop from transformation of aragonitic sediments. Volery et al. (2009, 2010) concluded that the Clino fabrics described by Melim et al. (2002) and Munnecke et al. (1997) are very different from their fabrics. We suggest, however, that the fabrics described in sections 4 and 5 are similar to those described by Volery et al. (2009, 2010ears), although their fabrics are Cretaceous in age and their sediment probably contained less aragonite then our Neogene sediments. In addition, Volery et al. (2009, 2010) concluded that microporous fabrics develop only in the meteoric diagenetic environment. However, Melim et al. (2001a, 2002) demonstrated that the Clino microporous fabrics described herein developed in the marine diagenetic environment. These observations place doubt on the assertion by Volery et al. (2009) that microporous fabrics form only in calcitic seas.

CONCLUSIONS

The dominant permeability control in this sample set is pore-throat size linked to crystal size. The transformation of minimicrite sediment to microspar increases crystal size, pore-throat size, and permeability without a significant change in porosity. The connecting pore space is intercrystal and is not clearly visible in thin sections. Therefore, it is considered to be microporous even though pore-throat sizes range from micro- to mesoscale.

We agree with previous authors that cementation is important in the formation of microspar development. However, we conclude that the transformation of minimicrite sediment to microspar is a replacement process, not simple cementation. Micrometer- and nanometer-scale aragonitic and calcitic minimicrite is dissolved and 1- to 10-µm microspar crystals precipitate in the volume previously occupied by minimicrite and in the associated pore space. Calcite not only replaces minimicrite crystals but also grows as cement in pore space that existed between minimicrite crystals. The volume of replacement calcite is balanced by the volume of carbonate dissolution. There is no outside source of carbonate. After most of the minimicrite has been replaced, cement grows in the intercrystal and vuggy pore

space of the microspar fabric. The carbonate is from an unknown outside source.

Simple dissolution is not a part of this diagenetic process. In the early stages of development, porosity is not related to a simple dissolution event but is inherited from the precursor fabric. Pore space is redistributed and pore-throat size modified through a replacement process. Later, porosity is lost through cementation, and petrophysical properties are reduced accordingly.

Needle- and rod-shaped crystals are plastered on the surface of growing calcite crystals and interfere with crystal growth, resulting in uneven, anhedral, crystal facies. The aragonite crystals are not embedded in microspar. Previous authors, viewing SEM images of broken surfaces, may well have misinterpreted the uneven crystal faces to be embedded aragonite crystals

A key observation in this study is that measured porosity does not change significantly during the transformation of minimicrite to microspar, an observation that supports the conclusion that the initial transformation is a replacement process and not cementation. This observation illustrates the importance of linking measured porosity, permeability, and pore size data to thin section and SEM descriptions for an improved understanding of carbonate diagenetic processes.

ACKNOWLEDGMENTS

This research was funded by the many industrial members of the Carbonate Reservoir Characterization Research Laboratory of the Bureau of Economic Geology, Jackson School of Geosciences, University of Texas at Austin. The authors would like to thank Gregor Eberli, Peter Swart, and Robert Ginsburg for permission to sample the Clino core. SEM photographs were taken by Robert Reed and Patrick Jones of the BEG. MICP data were provided by Exxon Mobil Corporation courtesy of Shawn Fullmer. Comments by L. A. Melim, A. Munnecke, and Nereo Preto, and by reviewers Shawn Fullmer and Lowell Waite were very helpful. The paper was edited by Chris Parker and Lana Dieterich. Publication authorized by the Director, Bureau of Economic Geology.

REFERENCES CITED

Cantrell, D. L., and R. M. Hagerty, 1999, Microporosity in Arab Formation carbonates, Saudi Arabia: GeoArabia. v. 4, p. 129–154.

Dravis, J. J., 1989. Deep-burial microporosity in Upper Jurassic Haynesville oolitic grainstones, East Texas, *in* C. R. Handford, R. G. Loucks, and S. O. Moshier, eds., Nature and origin of microrhombic calcite and associated microporosity in carbonate strata: Sedimentary Geology, Special Issue, v. 63, p. 325–341.

Folk, R. L., 1965, Some aspects of recrystallization in ancient limestones, *in* L. C. Pray and R. C. Murray, eds., Dolomitization and limestone diagenesis: A symposium: Society of Economic Paleontologists and Mineralogists Special Publication 13, Tulsa, Oklahoma, p. 14–48.

Folk, R. L., 1974, The natural history of crystalline calcium carbonate: Effect of magnesium content and salinity: Journal of Sedimentary Petrology, v. 44, p. 40–53.

Ginsburg, R. N., 2001, Subsurface geology of a prograding carbonate platform margin, Great Bahama Bank: Results of the Bahamas drilling project: Society of Economic Paleontologists and Mineralogists Special Publication 70, Tulsa, Oklahoma, 271 p.

Goldhammer, R. K., 1997, Compaction and decompaction algorithms for sedimentary carbonates: Journal of Sedimentary Research, v. 67, p. 26–35.

Heasley, E. C., R. H. Worden, and J. P. Hendry, 2000, Cement distribution in a carbonate reservoir: Recognition of a palaeo oil–water contact and its relationship to reservoir quality in the Humbly Grove Field, onshore, United Kingdom: Marine and Petroleum Geology, v. 17, p. 639–654.

Jameson, J., 1994, Models of porosity formation and their impact on reservoir description, Lisburne Field, Prudhoe Bay, Alaska: American Association of Petroleum Geologists Bulletin, v. 78, p. 1651–1678.

Kenter, J. A. M., R. N. Ginsburg, and S. R. Troelstra, 2001, Sea-level-driven sedimentation patterns on the slope and margin, *in* R. N. Ginsburg, ed., Subsurface geology of a prograding carbonate platform margin, Great Bahama Bank: Results of the Bahamas drilling project: Society of Economic Paleontologists and Mineralogists Special Publication 70, Tulsa, Oklahoma, p. 61–100.

Lambert, L., C. Durlet, J.-P. Loreau, and G. Marnier, 2006, Burial dissolution of micrite in Middle East carbonate reservoirs (Jurassic-Cretaceous): Keys for recognition and timing: Marine and Petroleum Geology, v. 23, p. 79–92.

Lasemi, Z., and P. A. Sandberg, 1984, Transformation of aragonite-dominated lime muds to microcrystalline limestones: Geology, v. 12, p. 420–423.

Lucia, F. J., 1995, Rock-fabric/petrophysical classification of carbonate pore space for reservoir characterization: American Association of Petroleum Geologists Bulletin, v. 79, p. 1275–1300.

MacIntyre, I. G., and R. P. Reid, 1995, Crystal alteration in a living calcareous alga (*Halimeda*): Implications for studies in skeletal diagenesis: Journal of Sedimentary Research, v. A65, p. 143–153.

MacIntyre, I. G., and R. P. Reid, 1998, Recrystallization in living porcelaneous foraminifera (*Archaias angluatis*): Textural changes without mineralogic alteration: Journal of Sedimentary Research, v. 68, p. 11–19.

McManus, K. M., and F. D. Rimstidt, 1982, Aqueous aragonite to calcite transformation: A geometry controlled dissolution-precipitation reaction (abs.): Geological Society of America Abstracts with Programs, v. 14, p. 562.

McNeill, D. F., G. P. Eberli, B. H. Lidz, P. K. Swart, and J. A. M. Kenter, 2001, Chronostratigraphy of a prograded carbonate platform margin: A record of dynamic slope sedimentation, Western Great Bahama Bank, *in* R. N. Ginsburg, ed., Subsurface geology of a prograding carbonate platform margin, Great Bahama Bank: Results of the Bahamas drilling project: Society of Economic Paleontologists and Mineralogists Special Publication 70, Tulsa, Oklahoma, p. 101–136.

Melim, L. A., P. K. Swart, and R. G. Maliva, 2001a, Meteoric and marine-burial diagenesis in the subsurface of Great Bahama Bank, *in* R. N. Ginsburg, ed., Subsurface geology of a prograding carbonate platform margin, Great Bahama Bank: Results of the Bahamas drilling project: Society of Economic Paleontologists and Mineralogists Special Publication 70, Tulsa, Oklahoma, p. 137–161.

Melim, L. A., F. S. Anselmetti, and G. P. Eberli, 2001b, The importance of pore type on permeability of Neogene carbonates, Great Bahama Bank, *in* R. N. Ginsburg, ed., Subsurface geology of a prograding carbonate platform margin, Great Bahama Bank: Results of the Bahamas drilling project: Society of Economic Paleontologists and Mineralogists Special Publication 70, Tulsa, Oklahoma, p. 217–238.

Melim, L. A., H. Westphal, P. K. Swart, G. P. Eberli, and A. Munnecke, 2002, Questioning carbonate diagenetic paradigms: Evidence from the Neogene of the Bahamas: Marine Geology, v. 185, p. 27–53.

Moshier, S. O., 1989, Microporosity in micritic limestones, a review, *in* C. R. Handford, R. G. Loucks, and S. O. Moshier, eds., Nature and origin of microrhombic calcite and associated microporosity in carbonate strata: Sedimentary Geology, Special Issue, v. 63, p. 191–213.

Moshier, S. O., and K. M. McManus, 1986, Textural evolution during lime mud diagenesis (abs.): American Association of Petroleum Geologists Bulletin, v. 70, p. 623–624.

Munnecke, A., H. Westphal, J. J. G. Reijmer, and C. Samtleben, 1997, Microspar development during early marine burial diagenesis: A comparison of Pliocene carbonates from the Bahamas with Silurian limestone from Gotland (Sweden): Sedimentology, v. 44, p. 977–990.

Pittman, E. D., 1992, Relationship of porosity and permeability to various parameters derived from mercury injection-capillary

pressure curves for sandstone: American Association of Petroleum Geologists Bulletin, v. 72, p. 191–198.

Rendle, R. H, and J .J. G. Reijmer, 2002, Quaternary slope development of the western, leeward margin of the Great Bahama Bank: Marine Geology, v. 185, p. 143–164.

Volery, C., E. Davaud, C. Durlet, B. Clavel, J. Charollais, and B. Caline, 2010, Microporous and tight limestones in the Urgonian Formation (late Hauterivian to early Aptian) of the French Jura Mountains: Focus on the factors controlling the formation of microporous facies: Sedimentary Geology, v.230, p. 21–34.

Volery, C., E. Davaud, A. Foubert, and B. Caline, 2009, Shallow marine microporous carbonate reservoir rocks in the Middle East: Relationship with sea water Mg/Ca ratio and eustatic sea-level: Journal of Petroleum Geology, v. 32, p. 313–325.

Westphal, H., M. J. Head, and A. Munnecke, 2000, Differential diagenesis of rhythmic limestone alterations supported by palynological evidence: Journal of Sedimentary Research, v. 70, p. 715–725.